

AERODYNAMICS AND AEROACOUSTIC ANALYSIS OF A SUPERSONIC SLENDER-BODY GEOMETRY

Maria De Rosa¹, Antimo Glorioso¹, Giuseppe Pezzella¹ & Antonio Viviani¹

¹Dipartimento di Ingegneria, Università degli Studi della Campania "Luigi Vanvitelli", Aversa (CE), 81031, Italy

Abstract

This paper deals with the investigation of the sonic boom phenomenon for a slender-body fuse geometry. The research effort focuses on the impact of a shape parameter, namely nose radius-to-diameter ratio $\frac{r}{D}$, in order to investigate its effects on the aerodynamics and aeroacoustics of the body in both the near and far-field domains. The first part of this work is done using computational fluid dynamics and considering the three-dimensional space to examine the pressure signature of the body in the near-field. Three different stations moving away from the center-line of the body, namely $(\frac{H}{L})_1$, $(\frac{H}{L})_3$, and $(\frac{H}{L})_5$ are considered. Additionally, the effect of the nose radius-to-diameter ratio on the aeroshape drag coefficient C_D is evaluated. The second phase of the research work involves studying the propagation of the pressure signatures using the NASA PC-Boom code. Parameters such as amplitude and wavelength are analysed to assess how the ratio $\frac{r}{D}$ affects the ground-level solution.

Keywords: Aeroacoustics; Noise; Sonic Boom; CFD; Propagation.

1. Introduction

As a result of the interest in the supersonic flight, the minimization of the acoustic phenomenon which happens when the aircraft flies at a speed greater than sound, known as sonic boom, has become a widely studied topic in recent years. High speeds produce high pressure disturbance, which result in a series of shock and expansion pressure waves in the aircraft's near-field [1]. When propagated to the ground through the atmosphere, these waves coalesce into an N-wave, whose name derives from the characteristic shape of the wave, see Fig. 1 [2]. The scientists' interest in this study is due to the fact that the supersonic flight overland was prohibited by Authorities as Federal Aviation Administration (FAA) because of the noise associated to this wave [3], which intensity increases with the over-pressure of the N-wave itself.

For the reasons above, this research paper focused on investigating the intensity of these shock waves and the associated sonic boom in the near-field, around some different configurations of an axi-symmetric slender-body geometry, namely AXIE [4].

In the first phase, the focus was on the near-field and CFD simulations were performed in three dimensional space, using the commercial code Ansys Fluent [5]. AXIE was studied by modifying its shape with several nose fillets designed with different ratios $\frac{r}{D}$, where r is the radius of the fillets and D is the maximum diameter of the body. Their effect on the solution was evaluated, in particular how the pressure signature changes moving away from the body. Aerodynamic investigations were also carried out, evaluating the drag coefficient C_D , to investigate how nose fillets affected the solution in terms of drag.

In the second phase, the pressure signatures obtained from the near-field analysis were used as input for propagation assessments by using the NASA PC-Boom code [6] [7]. This code solves the Burgers equation to predict the sonic boom ground footprints. Downstream of the propagation, as the pressure disturbance coalesces into a N-wave, evaluating the effect of fillets on the solution propagating to the ground was fundamental to understanding how the amplitude and ultimately the wavelength change accordingly. [8]

By combining the near-field and far-field analysis, this study provides valuable insights into the relationship between the body geometry and the sonic boom mitigation [9].

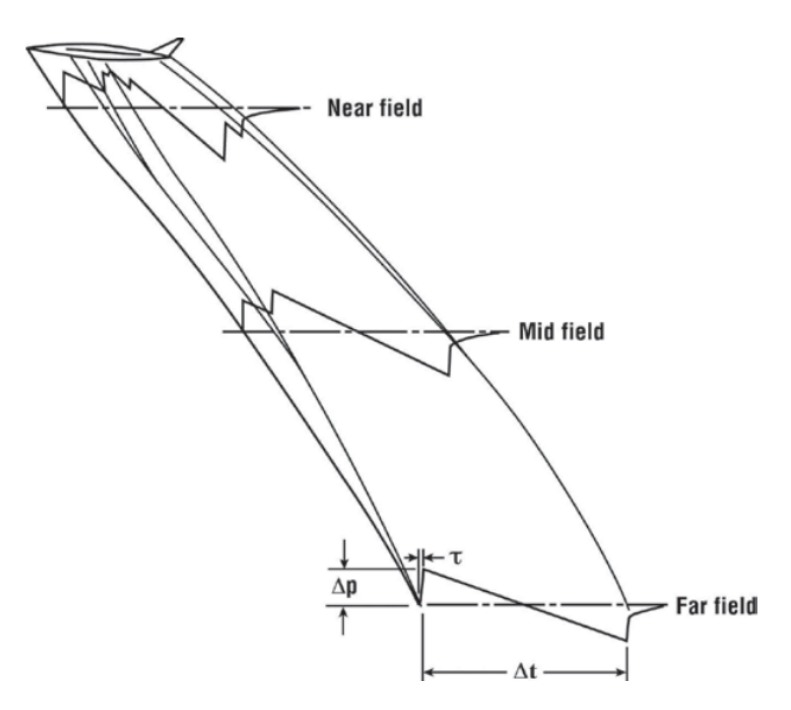


Figure 1 – Aeroacoustic domain and N-wave [2]

2. Numerical Approach

All simulations in near field are performed using the commercial Ansys Fluent [5] code. Ansys Fluent is based on unstructured finite-volume approach for solving the RANS, Reynolds-Averaged Navier-Stokes equations. ROE-FDS scheme[10] is used to investigate the aerodynamics and aeroacustics quantities. The pressure signature at three different locations away from the geometric centerline, specifically 1, 3 and 5 body lengths, is calculated. Green-Gauss approach is used to compute the gradients and an adaptive CFL number strategy was adopted. All simulations are performed using the inviscid Euler equations and the ideal gas model for air.

Finally, far field propagation is performed using PCBoom [6] [7], a NASA code for the propagation, born by the sonic boom program written by Thomas in the early 1970s [11].

3. Studied cases

The configurations analysed in this research effort are now briefly described. They are obtained starting by the AXIE body, a test case presented at the 2nd AIAA Sonic Boom Prediction Workshop [4], considering the effect of several nose fillets.

3.1 AXIE

The AXIE (Axisymmetric Equivalent Area), Fig. 2, is an axisymmetric body designed by a full revolution around the x-axis. Despite its simplicity, it is interesting for aeroacoustic studies because it has the same pressure signature at the station $(\frac{H}{L})_3$ as NASA supersonic concept aircraft, namely C25D [12]. Its development has been the result of an inverse design process described by Anderson [13]. The AXIE reference length is 32.92m and its operating conditions are Mach equal to 1.6 at an altitude of 15760 m, see Tab. 1.

3.2 AXIE Shaped configurations

Five different configurations are designed by increasing the nose radius-to-diameter ratio $\frac{r}{D}$ from 0% to 10% to investigate the effects of the fillets on the sonic boom signature. A zoom view of the resultant configurations is shown in Fig. 3 and the details of the fillets are summarized in Tab. 2.

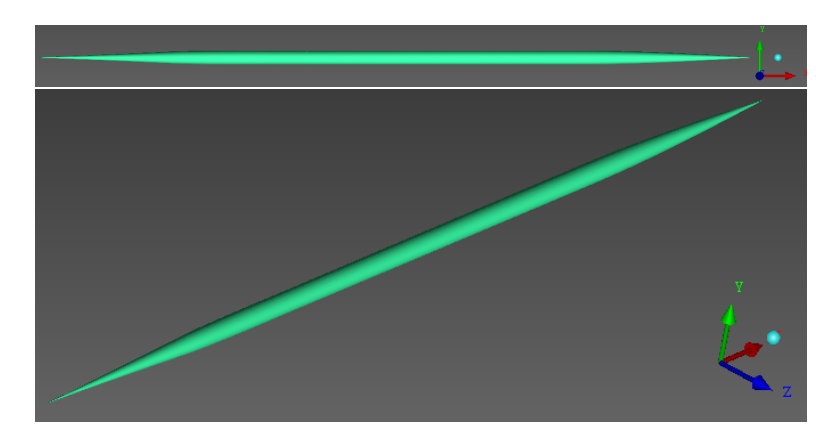


Figure 2 – AXIE Geometry

Table 1 - AXIE operating conditions

Operating conditions	Value
Mach number	1.6
Angle of attack [deg]	0
Altitude [m]	15760.0
Pressure [Pa]	10684.3
Temperature [K]	216.6

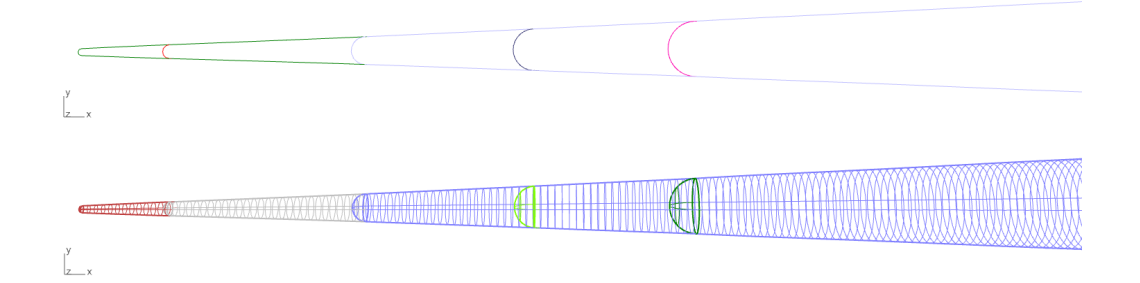


Figure 3 – AXIE and the different $\frac{r}{D}$ ratio in series

Table 2 - Fillets geometric characteristics

$\frac{r}{D}$ [%]	R [mm]
2.5	15.774
5	31.548
10	63.097
15	96.645
20	126.193

4. Near-field CFD Approach and Results

4.1 Grid Generation

In order to study the aeroacoustics of all configurations under investigation, several computational meshes are generated. They are designed according to the methodology presented in Ref.s [14], [15], [16], by exploiting a hybrid approach that combines an internal unstructured grid with an external structured one, whose cells are aligned with the freestream Mach-wave angle[17], μ .

Grids of about 10M cells (half body) are obtained for each case, a zoom of which is shown in Figure 4, while the domain is shown in Figure 5.

All simulations are performed under the same operating conditions, which are summarised in Tab. 1.

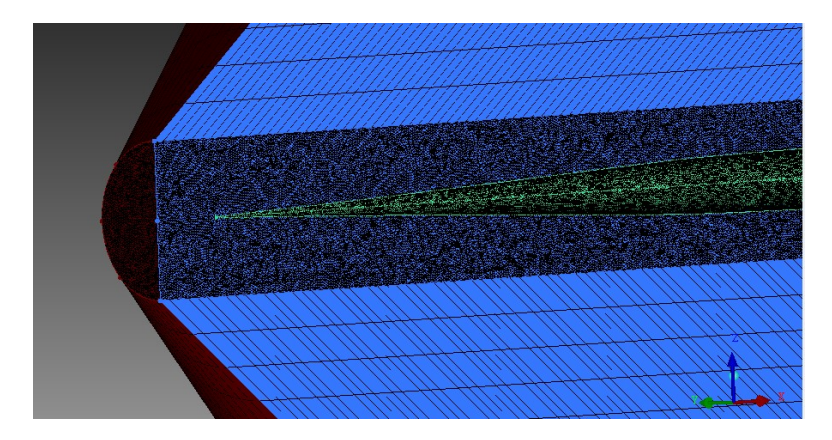


Figure 4 – 3D Aeroacoustic Mesh: 10M cells

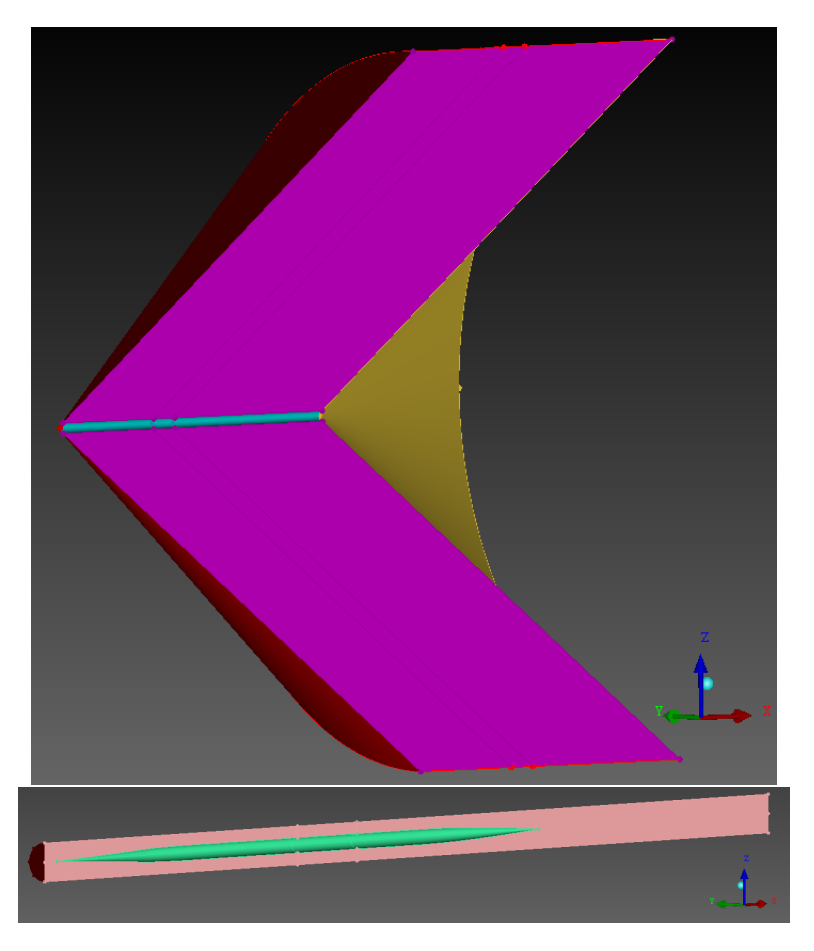


Figure 5 – 3D Aeroacoustic Domain Geometry: structured domain up, unstructured domain down

4.2 Numerical Results

This section contains the pressure signatures of both the AXIE body and the configurations derived by it through nose filleting. The pressure signature $\frac{dp}{p}$ reads:

$$\frac{dp}{p} = \frac{p_s - p}{p} \tag{1}$$

In Eq.(1), p_s is the local static pressure for each point along the line where signature is extracted, while p is the free-stream static pressure.

The pressure signature is extracted in correspondence of three stations, namely $(\frac{H}{L})_1$, $(\frac{H}{L})_3$, and $(\frac{H}{I})_5$, shown in Figure 6.

Aerodynamics and aeroacoustics analysis of a supersonic slender-body geometry

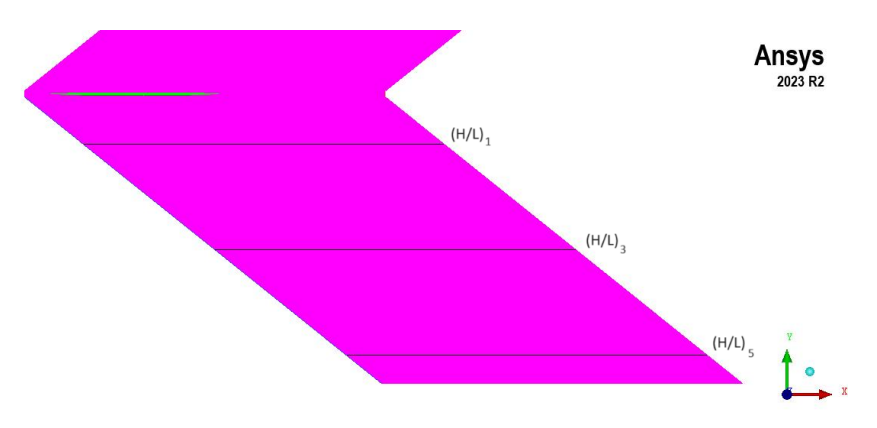


Figure 6 – Stations of the extracted pressure signatures

Pressure signatures recorded at each station $\frac{H}{L}$ are shown in the following Figure 7 and Figure 8.

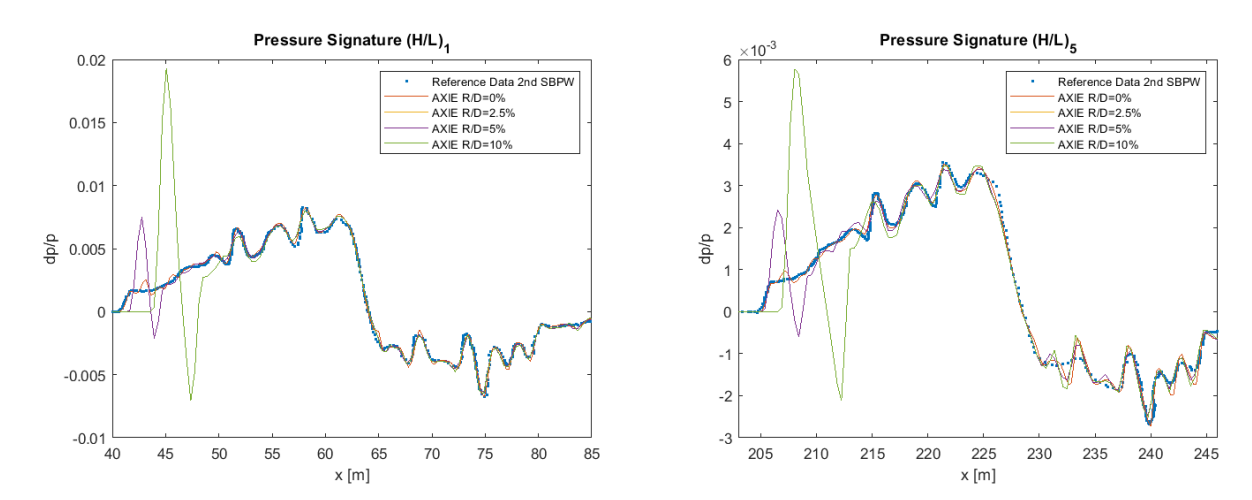


Figure 7 – Near-field pressure signature station $(\frac{H}{L})_1$ and $(\frac{H}{L})_5$

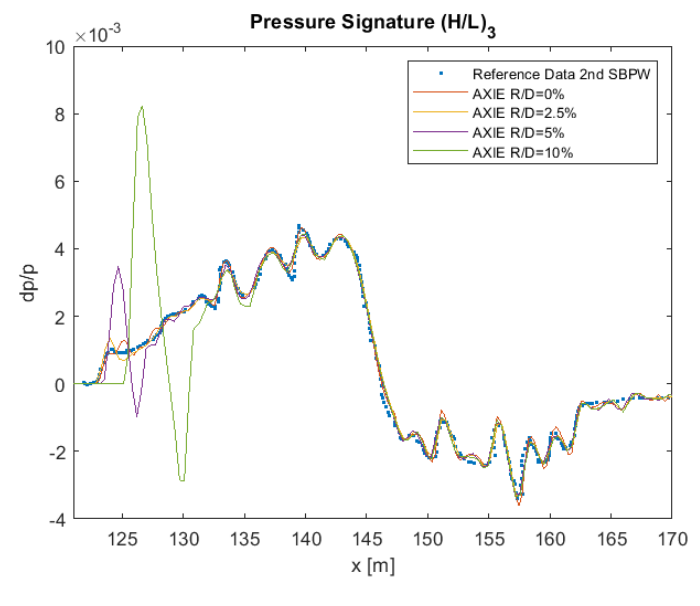


Figure 8 – Near-field pressure signature station $(\frac{H}{L})_3$

The reference data are taken from the Second Sonic Boom Prediction Workshop and are represented

by the dot-marker symbol [18]. As can be seen from the plots, there is a good agreement between the results of the $\frac{r}{D}=0\%$ AXIE configuration and the reference data. However, when looking at the results of the configurations with the fillets, a clear difference can be observed in the first part of the signature, while the second part matches the reference data. This difference is due to strong bow shock at nose of the body since the introduction of fillets, and increases as the nose radius-to-diameter ratio $\frac{r}{D}$ increases.

Since the evident difference between the $\frac{R}{D} = 0\%$ and $\frac{r}{D} = 10\%$ configurations, results of the other two bodies are not presented for brevity.

The fillet effects are also illustrated in Fig. 9, where contours of Mach number on the symmetry plane are shown. These contours shows the series of shock and expansion waves in the aircraft's near-field. The shock at nose become more pronounced as the nose radius-to-diameter ratio increases, in accordance with pressure signatures. That result is more evident in the contour of the configuration with $\frac{r}{D} = 10\%$, where a strong shock is well highlighted.

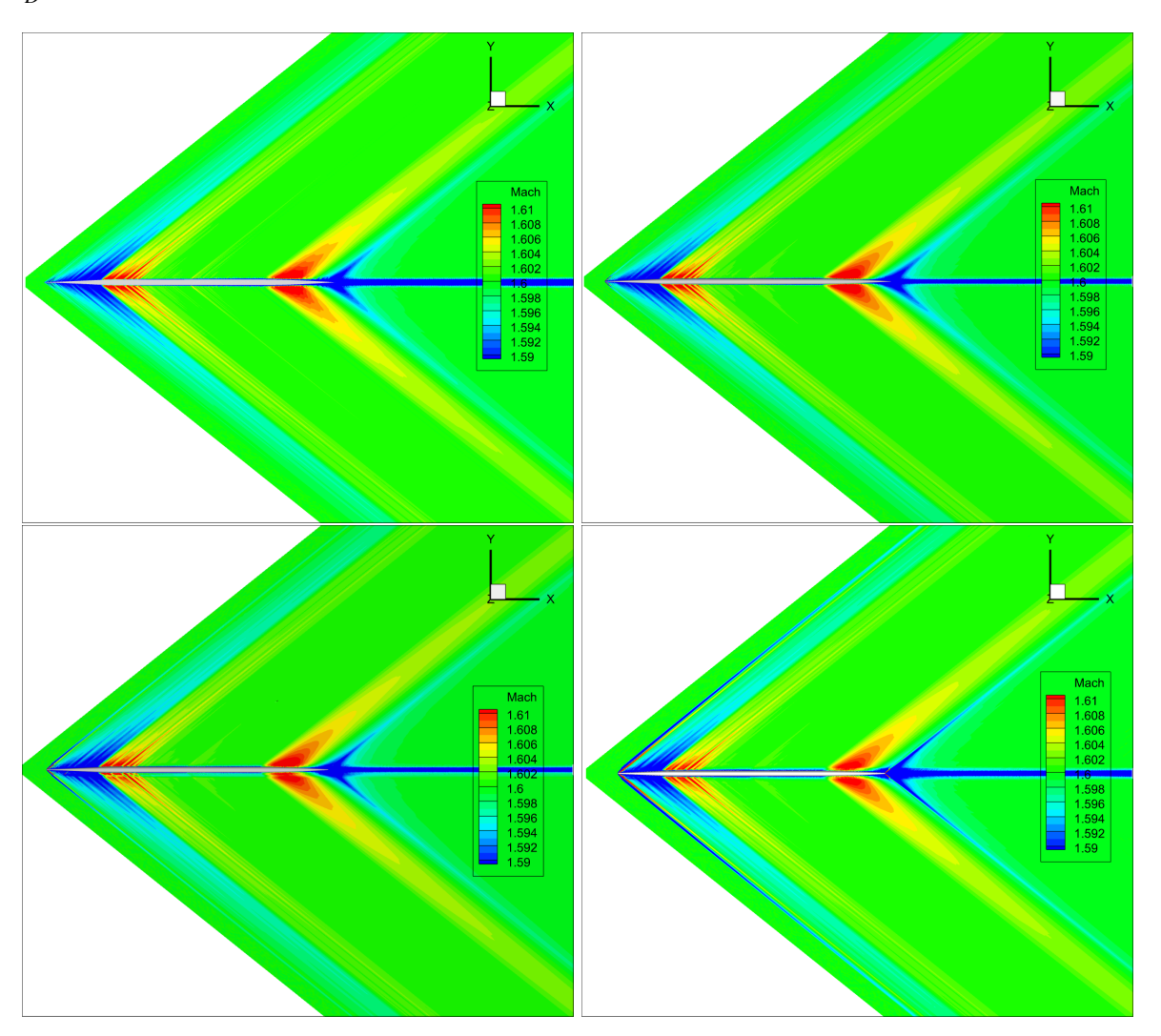


Figure 9 – Contours of Mach number - top left $\frac{r}{D}=0\%$, top right $\frac{r}{D}=2.5\%$, bottom left $\frac{r}{D}=5\%$, bottom right $\frac{r}{D}=10\%$

The drag coefficient is evaluated as well and the obtained values are listed in Table 3, a percentage difference is calculated too, S_{ref} is the maximum cross-sectional area $A_{cross}=0.31m^2$. Figure 10 shows the increase of C_D versus $\frac{r}{D}$ in relation to the slenderness of the body, $\frac{L}{D}$, which is listed in the legend. The coefficient increases with the growth of the fillet's ratio, due to the amplification of the shock on the nose itself. In particular, for the configuration with a fillet of $\frac{r}{D}=10\%$, the obtained C_D is 283% greater than the $\frac{r}{D}=0\%$ (i.e., reference body).

Table 3 – AXIE C_D values

$\frac{r}{D}$	C_D	Difference [%]
0%	0.00806	0
2.5%	0.01405	74.3
5%	0.01702	111
10%	0.03094	283

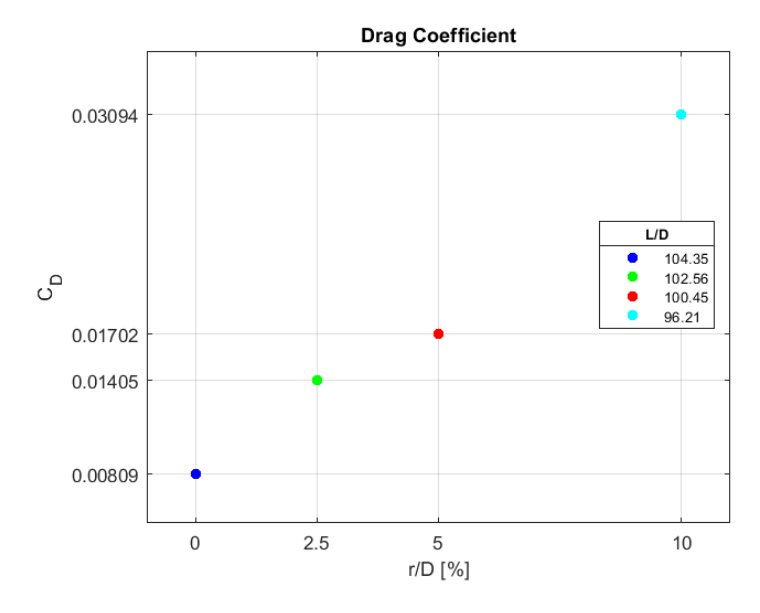


Figure 10 – Evaluation of the drag coefficient for all configurations

5. Far-field and Propagation Results

The pressure signatures obtained in the previous paragraph are propagated to the ground using the NASA PC-Boom code [19]. In particular, the signature obtained at $(\frac{H}{L})_3$ in the preceding section is propagated. Propagation is performed using the mandatory atmospheric profile given to participants at the Second Sonic Boom Prediction Workshop [8], "Profile3", whose temperature, X-wind, Y-wind and relative humidity details are shown in Figure 11 as [T3,WX3,WY3,RH3], respectively.

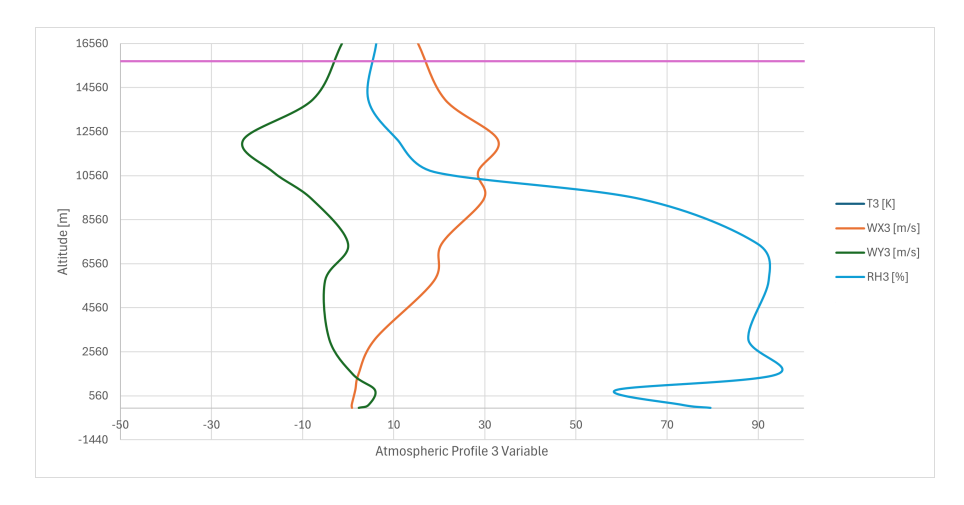


Figure 11 – Atmospheric profile from the Second Sonic Boom Prediction Workshop

In this atmospheric profile, the values of temperature and pressure are taken from the U.S. Standard Atmosphere [20], while the relative humidity is chosen from ANSI S1.26, Annex C guidance [21] [8]. The first stage of the analysis is carried out using the pressure signature in near-field provided in the workshop [18] and the evaluated parameter is the overpressure on ground.

The ground signature obtained is compared with the result of propagation of one participant in the

workshop, particularly P11. A perfect match is shown in the Figure 12.

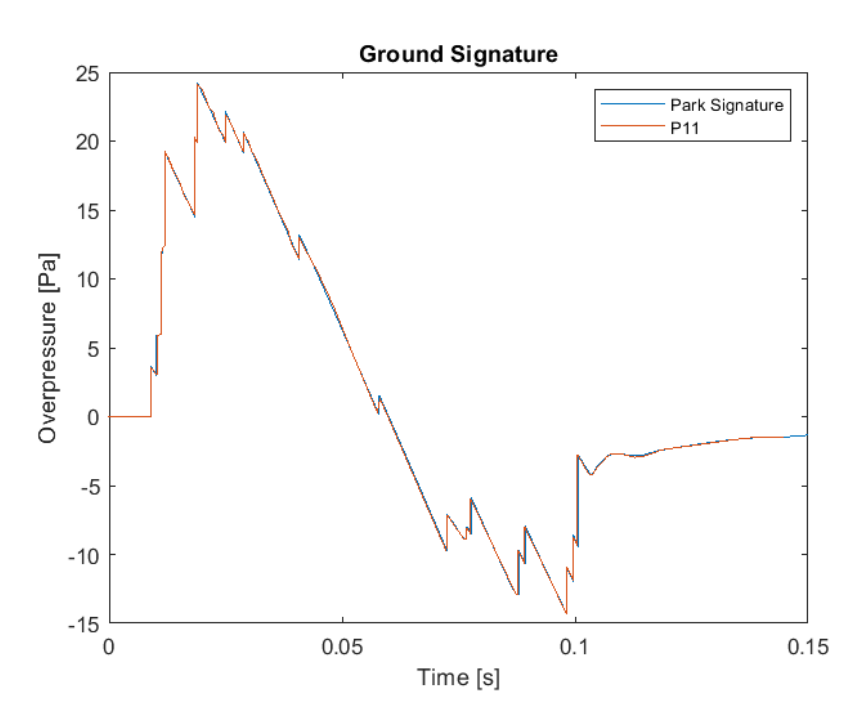


Figure 12 – Ground signature comparison

In the second stage of the analysis, pressure signatures in near-field are propagated at ground. Fig. 13 shows the results. As it is evident, when compared to the $\frac{r}{D}=0\%$ configuration, due to the presence of the fillets the measured overpressure first increases and then decreases. In terms of time, the compression associated with the ground signature has an earlier onset and therefore a longer duration. These effects become more pronounced as the nose-to-radius ratio $\frac{r}{D}$ of the fillets increases. From a global view of the events, it can be said that despite the first pronounced peak of the overpressure, the maximum value of the overpressure decreases with the fillets. Anyway, it is worth recalling that the larger the nose radius, the greater the aerodynamic drag for the body.

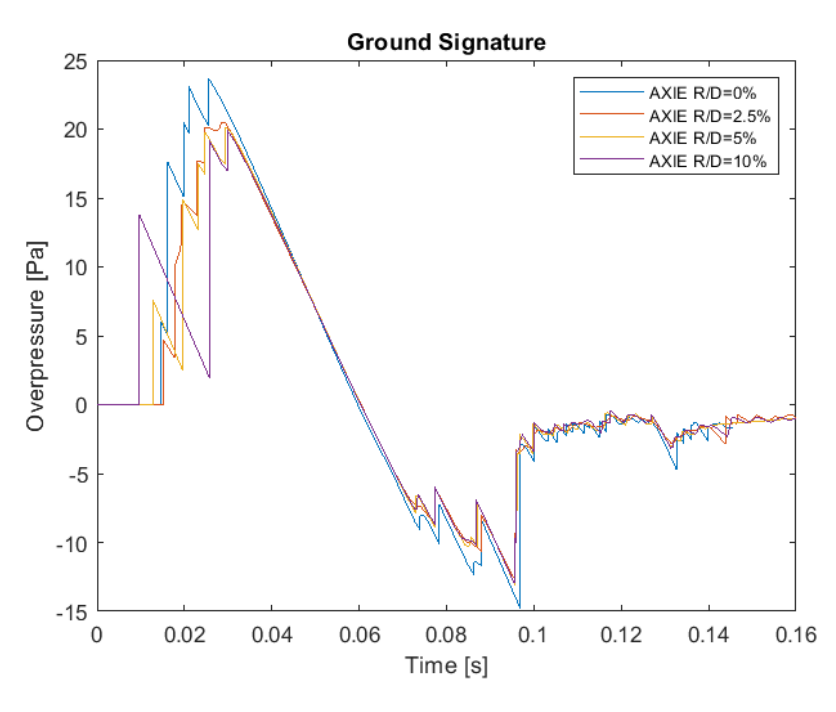


Figure 13 – Ground signature of the different configurations

6. Conclusions

In this work, near-field and far-field analyses are performed to study the sonic boom phenomenon and to predict the associated ground signature. In particular, the near-field domain is modelled by the Euler equations with CFD simulations in ANSYS Fluent, while far-field propagation studies were performed with NASA PC-Boom. Based on an axisymmetric body of revolution, AXIE, a shape parameter, the nose radius-to-diameter $\frac{r}{D}$, is considered to study its aerodynamic and aeroacoustic effects on the near-field pressure and ground signatures. The results obtained show a clear influence of the fillets on the signature characteristics, in both domains. In detail, the near-field pressure signature reveals an increasing shock at the nose, which intensifies as the ratio $\frac{r}{D}$ increases. Due to the increasing shock, the drag coefficient also grows, reaching a value 283% greater for the configuration with a fillet of $\frac{r}{D}=10\%$ compared to the $\frac{r}{D}=0\%$ case.

The fillets have an impact on the characteristics of the ground signature, too. Solutions obtained show that the overpressure first increases and then decreases as the ratio $\frac{r}{D}$ increases. Overall, the value of the maximum overpressure decrease with the fillet.

When analysing the far-field results, it seems convenient to adopt $\frac{r}{D}=2.5\%$ and $\frac{r}{D}=5\%$ fillets, since no significant increase is visible in the pressure peaks at the ground, different from the result of the $\frac{r}{D}=10\%$ fillet, where a strong increase is visible in the initial part of the pressure signature. It is different when analysing the near-field results. A rise in the pressure peaks is visible for each fillet and a large increase in C_D is evident, Tab. 3, where the percentage increase starts from 74% to reach 283% in relation to the case without any fillet. Considering the whole life cycle of an aircraft, the increase is very important to take into account the fillet to reduce the noise on the ground in supersonic fields.

7. Contact Author Email Address

Mail to: giuseppe.pezzella@unicampania.it

8. Copyright Statement

The authors confirm that they, and/or their company or organization, hold copyright on all of the original material included in this paper. The authors also confirm that they have obtained permission, from the copyright holder of any third party material included in this paper, to publish it as part of their paper. The authors confirm that they give permission, or have obtained permission from the copyright holder of this paper, for the publication and distribution of this paper as part of the ICAS proceedings or as individual off-prints from the proceedings.

References

- [1] D. J. Maglieri H. W. Carlson. Review of sonic-boom generation theory and prediction methods. 1972.
- [2] et al. Domenic J. Maglieri. In SONIC BOOM, Six Decades of Research. NASA, SP-2014-622, 2014.
- [3] FAA. Civil aircraft sonic boom.
- [4] Michael A. Park and Marian Nemec. Nearfield summary and statistical analysis of the second aiaa sonic boom prediction workshop. Journal of Aircraft, 56(3):851–875, 2019.
- [5] Ansys Fluent Fluid Simulation Software. ANSYS, Inc., release 18.1 edition, 2018.
- [6] Joel B. Lonzaga. Recent enhancements to nasa's poboom sonic boom propagation code. AIAA Aviation 2019 Forum, 2019.
- [7] Bruno Koobus Mariano Vázquez, Alain Bernard Dervieux. A methodology for the shape optimization of flexible wings. Engineering Computations, pages 344–367, 2006.
- [8] Alexandra Loubeauy Sriram K. Rallabhandi. Summary of propagation cases of the second aiaa sonic boom prediction workshop. 2017.
- [9] Qian Zhansen Lengyan. A cfd based sonic boom prediction method and investigation on the parameters affecting the sonic boom signature. 2015.
- [10] P L Roe. Characteristic-based schemes for the euler equations. <u>Annual Review of Fluid Mechanics</u>, 18(1):337–365, 1986.
- [11] Juliet A. Page, Joel B. Lonzaga, Meghan J. Shumway, Sophie R. Son, Robert S. Downs, Alexandra Loubeau, and William J. Doebler. PCBoom Version 7.3 User's Guide.
- [12] James W. Fenbert Mathias Wintzer, Irian Ordaz. Under-track cfd-based shape optimization for a low-boom demonstrator concept. 33rd AIAA Applied Aerodynamics Conference, AIAA Paper, 2015.
- [13] George R.Anderson. SHAPE OPTIMIZATION IN ADAPTIVE SEARCH SPACES.

Aerodynamics and aeroacoustics analysis of a supersonic slender-body geometry

- [14] Alaa Elmiligui Michael A. Park, Richard L. Campbell. Specialized cfd grid generation methods for near-field sonic boom prediction. AIAA Paper, 201a.
- [15] Michael J. Aftosmis Mathias Wintzer, Marian Nemec. Adjoint-based adaptive mesh refinement for sonic boom prediction. 26th AIAA Applied Aerodynamics Conference, AIAA paper, 2008.
- [16] A. Glorioso, F. Petrosino, A. Aprovitola, M. Barbarino, G. Pezzella, and A. Viviani. Sonic boom generation using open source cfd approach. AIAA AVIATION 2023 Forum, 2023.
- [17] J.-M. Moschetta and J. Gressier. The sonic point glitch problem: A numerical solution. 1998.
- [18] Asa 2022 special focus boom session. https://lbpw-ftp.larc.nasa.gov/sbpw2/, 2022. Accessed: 2024.
- [19] Sophie Kaye Robert S. Downs and Juliet A. Page. Sonic boom prediction workshop 3: Propagation modeling using pcboom. 2020.
- [20] U.S. Government Printing Office. U.S. Standard Atmosphere, 1976.
- [21] American National Standards Institute New York NY Committee S1, Acoustics. <u>ANSI Standard S1.26-1995, 1995.</u>